International Journal of Microwave and Wireless Technologies

cambridge.org/mrf

Low-profile high gain circularly polarized CRLH transmission line inspired antenna with artificial magnetic conductor for wearable applications

Mohammad Hussain Abbas[1], Shamsher Singh[1], Ankit Sharma[2] and Deepak Gangwar[3]

[1]Department of ECE, UIET, Maharshi Dayanand University, Rohtak, India; [2]Department of ECE, Galgotias College of Engineering and Technology, Greater Noida, India and [3]Department of ECE, Bharati Vidyapeeth's College of Engineering, New Delhi, India

Research Paper

Cite this article: Abbas MH, Singh S, Sharma A, Gangwar D (2023). Low-profile high gain circularly polarized CRLH transmission line inspired antenna with artificial magnetic conductor for wearable applications. *International Journal of Microwave and Wireless Technologies* **15**, 1223–1232. https://doi.org/10.1017/S1759078722001258

Received: 6 June 2022
Revised: 14 October 2022
Accepted: 19 October 2022

Key words:
Artificial magnetic conductor; circular polarization; CRLH TL; wearable antenna

Author for correspondence:
Deepak Gangwar,
E-mail: er.deepakgangwar@gmail.com

Abstract

In this work, a compact, wideband, circularly polarized wearable antenna is proposed using asymmetric coplanar strip feeding for wireless health monitor applications in the ISM frequency band. The proposed antenna consists of a composite right/left transmission line (CRLH TL) inspired structure to achieve compactness and a rectangular ring slot is created in the metallic ground to enhance the CP radiation of the antenna. A 5×5 artificial magnetic conductor unit cell-based metasurface is designed which is operating at 2.4 GHz as a ground plane for the CRLH-based CP antenna. Implementation of AMC-based metasurface as a ground plane results in enhancement of radiation characteristics of CRLH TL antenna. The proposed antenna has a small footprint of 50×50 mm^2 with measured impedance bandwidth of 2.3–3.2 GHz. The 3 dB axial ratio bandwidth of the proposed antenna is 2.36–2.78 GHz with peak gain of 5.89 dBi. Simulation and experimental results show that proposed AMC-based antenna is robust in terms of structural deformation. Further, to validate the performance of the antenna for biomedical applications, we have simulated the proposed antenna with human phantom model. The proposed antenna exhibits stable scattering and radiation characteristics with the phantom body environment and due to the inclusion of AMC structure, the proposed design satisfies maximum specific absorption rate value given as per the IEEE standard safety guidelines.

Introduction

Wireless body area network (WBAN) has been developing rapidly in the communication field [1, 2]. It has attracted attention of scientists and researchers because of its wide range of applications in military, sports, medical monitoring, and several other fields [3, 4]. Wearable antennas used in WBAN have particular criteria in terms of design and size as compared to conventional antennas, such as waist, neck, and arm-wearable antennas must be in the form of a belt or button [5–9]. As a result, enhancing the performance of wearable antennas is critical, particularly in the realm of telemedicine systems [5].

Monopole antennas are commonly utilized in the field of WBAN and are placed near to the human body, which results an impedance mismatching and a significant reduction in antenna radiation performance [10–14]. The electromagnetic band gap (EBG) and artificial magnetic conductor (AMC) based antennas proved to be great help in reducing the coupling effect of human body on the designed antennas [10, 15, 16]. Additionally, flexible AMC-based wearable antennas can help in reducing SAR value of the designed structure, which makes it simpler for researchers to develop antennas in accordance with human safety requirements [17–19]. In previous years, the design of AMC-based metasurface structures has focused on minimizing back lobe radiation, improving impedance bandwidth, enhancing antenna performance, and increasing gain. AMC-based metasurfaces also have the characteristics of a reflecting plane wave in the same phase and can achieve the performance of an ideal magnetic conductor in a definite frequency band [20–22]. Recently, an AMC-based low-profile wearable antenna for the ISM band with dimensions of 102×68 mm^2 and a peak gain of 6.12 dBi is presented [23]. A wearable monopole antenna consisting of tri-annular square ring with AMC is proposed for ISM, WBAN, and WiMAX applications. The proposed design works in the ISM [24]. A triple transmission line is used to improve the gain of wearable antenna operation in the dual band region of 1.7–2.5 and 5.4–5.95 GHz with gain value of 9.86 dBi with larger antenna dimension of $0.57\lambda \times 0.67\lambda$ [25]. Then, a two-element textile-based MIMO antenna is proposed with high isolation and polarization diversity. The proposed circularly polarized

© The Author(s), 2022. Published by Cambridge University Press in association with the European Microwave Association

antenna operates in the region of 3.3–4.3 GHz [26]. A circularly polarized UWB antenna is designed consisting of a metasurface structure with dual-band notch characteristics [27]. In [28] a miniaturized implantable antenna is proposed for ISM band applications. The proposed antenna exhibits impedance and axial ratio bandwidth (ARBW) of 2.25–2.78 and 2.32–2.63 GHz, respectively.

But the size of antenna is quite large. Thus, in the field of WBAN, wearable antenna plays an important role for wireless communication, and the performance of wearable antennas should not be degraded due to bending or crumpling. Hence it is necessary to design a miniaturized, low-cost wearable antenna with good radiation performance.

In this work, we have proposed and experimentally verified a low-profile CRLH-TL-based CP antenna combined with a miniaturized AMC structure for ISM band wearable applications. The paper is organized as follows: in section "Proposed antenna configuration and analysis" CRLH-TL-based antenna is designed and its equivalent circuit diagram is discussed. AMC unit cell structure is also designed and discussed in section "Proposed antenna configuration and analysis". Section "Proposed design integration of CRLH-based antenna and AMC" is based on the design and analysis of AMC integrated antenna. Section "Evaluation of AMC antenna performance under bending conditions" is dedicated to the discussion on the performance of AMC antenna for different bending conditions to evaluate the performance of antenna for wearable applications. Discussion on experimental results is done in section "Experimental results and discussion", and finally, conclusions are drawn in section "Performance of the proposed antenna on the human body".

Proposed antenna configuration and analysis

Antenna design

The schematic diagram of the CP antenna is shown in Fig. 1(a). The designed CPW fed CRLH-TL-based CP antenna is fabricated on Rogers RT duriod 5880 and it employs an asymmetric co-planar waveguide feeding strip scheme. The CRLH-based TL unit cell is realized on an *L*-shaped rectangular strip that serves as the antenna's feedline. The proposed antenna uses an asymmetric ground plane consisting of a rectangular-shaped slot. The equivalent circuit of the proposed structure based on CRLH-TL is shown in Figs 1(b) and 1(c). The *L*-shaped feed of the antenna gives the series inductance (L_r) of the CRLH-TL, as shown in Fig. 1(b), while a small rectangular ring slot will offer capacitance in series (C_l), forming the series arm (L_r and C_l) of the CRLH inspired TL. Further, rectangular strip attached to the feed line provides shunt inductance (L_l). The virtual ground

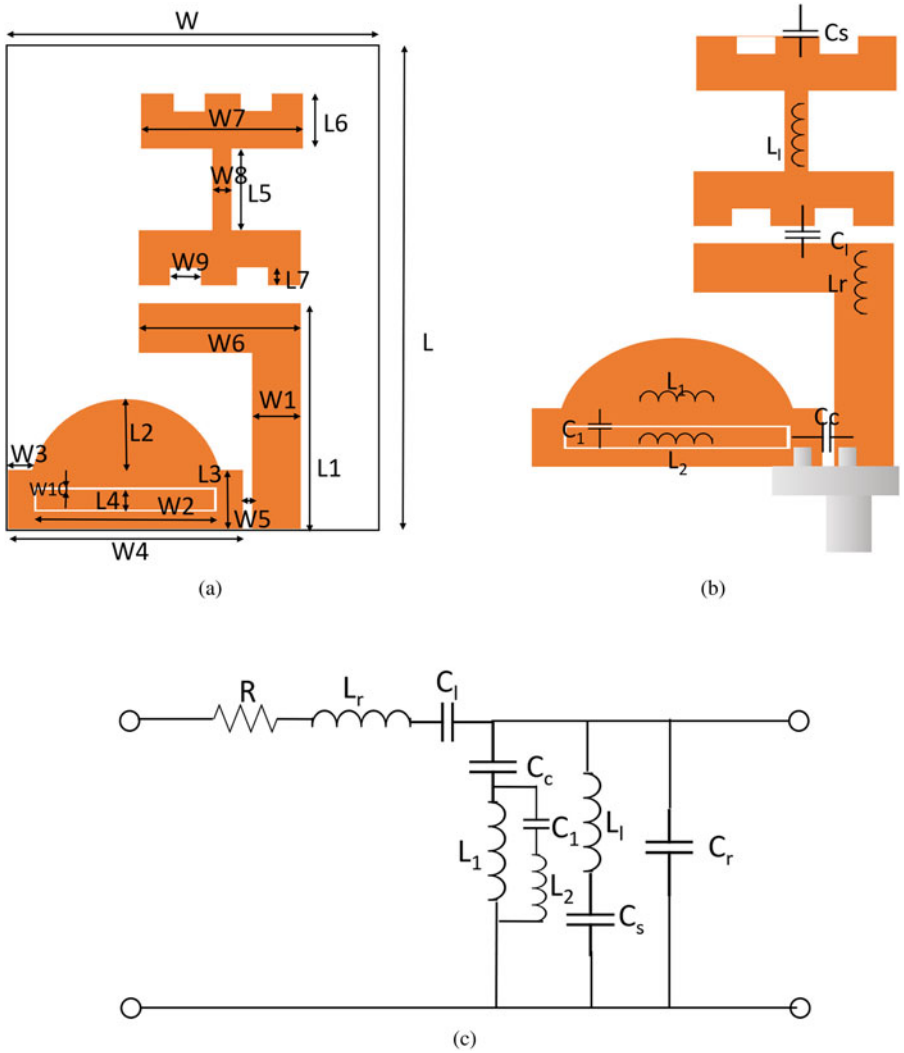

Fig. 1. (a) Top view of the antenna. (b) L-C representation of the antenna. (c) Equivalent circuit diagram of the antenna.

https://doi.org/10.1017/S1759078722001258 Published online by Cambridge University Press

for the shunt inductor is provided by the rectangular stub, which substitutes conventional CRLH-TL-based design concept of using shorted vias or metal posts for ground [29, 30]. The coupling capacitor C_c is formed by the gap w_5 between feed line and asymmetric ground plane. Further, coupling between the CRLH-TL and the ground plane supplies the shunt capacitor (C_r) that makes up the CRLH-TL shunt arm (L_l, C_s, C_c, and C_r). A rectangular annular ring slot with gap w_{10} is loaded in the ground plane to keep the antenna compact. A shunt tank circuit consisting of capacitor C_1 with inductors L_1 and L_2 is provided by a rectangular ring slot and ground plane as shown in Figs 1(b) and 1(c). CST Microwave Studio is used for antenna modeling and analysis. Table 1 shows the dimension of the proposed antenna.

Considering an open-ended TL condition, the input impedance calculated from one end of the resonator to the other is inversely proportional to the shunt admittance and number of unit cells. As a result, the resonant frequency of an open-ended ZOR antenna is identical to the shunt frequency, and it is only dependent on the shunt parameters [29, 30].

$$f_{zor} = f_{sh} = \frac{1}{2\sqrt{L_l\left[\frac{C_s(C_r + C_c)}{C_r + C_c + C_s}\right]}}. \quad (1)$$

Proposed AMC unit cell design and analysis

The configuration of AMC unit cell is shown in Fig. 2(a). The proposed AMC unit cell derived from EBG structure, and designed AMC consists of a circular patch with multiple rectangular slots. The AMC structure is designed on polyimide with a dielectric constant of 3.5, a loss tangent of 0.0027, and a thickness h_3 of 0.254 mm. The ground plane of the AMC structure is separated by $h_4 = 2.7$ mm. Figure 2(b) depicts reflection phase values of AMC unit cell. The AMC ±90° reflection phase

Table 1. Dimensions of the proposed antenna

Parameter	Value (mm)	Parameter	Value (mm)	Parameter	Value (mm)
L_1	15	W_1	4	a	10
L_2	4.6	W_2	13.7	a_1	9
L_3	4	W_3	1.49	b_1	1.4
L_4	1.5	W_4	17.9	r_1	4.8
L_5	9	W_5	0.3	r_2	1.5
L_6	5	W_6	10	r_3	0.5
L_7	1	W_7	10	h_1	0.8
L_8	50	W_8	0.9	h_2	10
L	40	W_9	2	h_3	0.254
W	27	W_{10}	0.25	h_4	2.7

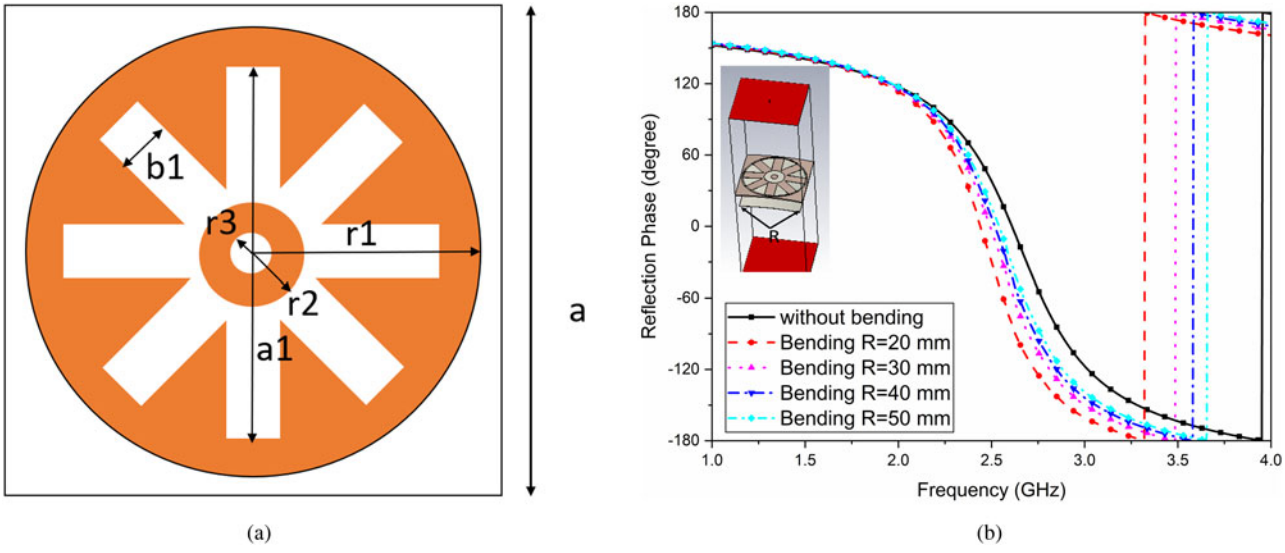

Fig. 2. (a) Top view of AMC unit cell. (b) Reflection phase of AMC unit cell under bent conditions.

https://doi.org/10.1017/S1759078722001258 Published online by Cambridge University Press

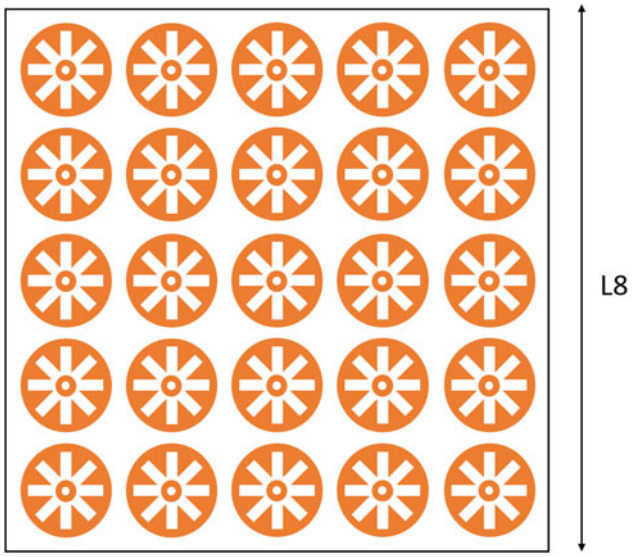

Fig. 3. Configuration of AMC-based metasurface.

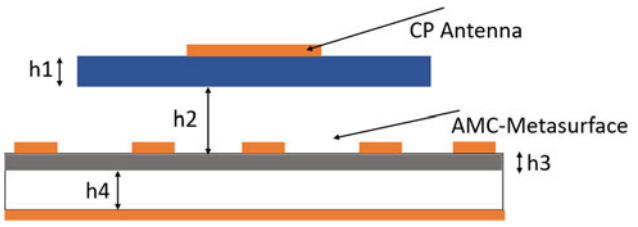

Fig. 4. Side view of CRLH-based CP antenna integrated with AMC.

bandwidth ranges from 2.1 to 2.8 GHz, with a 0° reflection phase at 2.5 GHz. To study the AMC for wearable applications, we have simulated reflection phase values at various degrees of bending and it is observed that the results of AMC unit cell is considerably good throughout a wide range of bending degrees. The AMC unit cell is durable and well-suited for wearable applications. The AMC metasurface shown in Fig. 3 is comprised of an array of 5×5 AMC unit cells.

Proposed design integration of CRLH-based antenna and AMC

Figure 4 depicts the side view of the proposed antenna, which is a combination of a CRLH-TL-based CP antenna and an AMC metasurface. A 5×5 AMC unit cell array is used as in-phase reflector to suppress the effect of the human body on the antenna and increase forward radiation. *S* parameter results of the antenna with and without AMC reflector are shown in Fig. 5(a). The impedance bandwidth of the antenna without AMC is 2.36–3.1 GHz, whereas the impedance bandwidth of the antenna with AMC is 2.3–3.1 GHz. It is observed that the resonance frequency of the AMC-loaded antenna is slightly shifted to the left side in comparison to the CRLH-based antenna. The simulated gain values of both antennas are shown in Fig. 5(b), with the AMC-loaded antenna exhibiting stable gain within the impedance bandwidth and a peak gain of

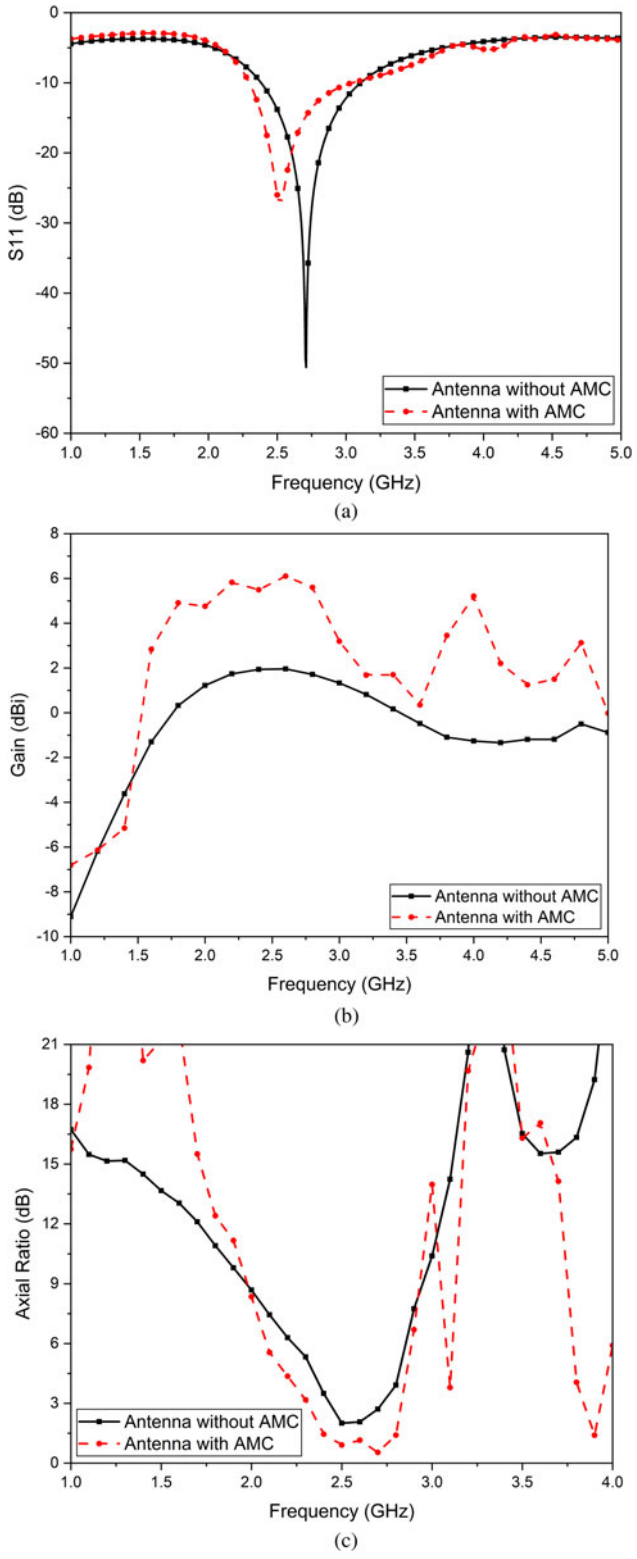

Fig. 5. Simulated (a) S_{11}. (b) Gain. (c) Axial ratio of antenna with and without AMC.

6.1 dBi at 2.6 GHz. It is also noticed that the AMC-loaded antenna (2.3–2.8 GHz) exhibits an improved 3 dB ARBW than the CRLH-TL-based antenna. As a result, we can conclude that combining AMC with the CRLH-TL-based CP antenna enhances overall radiation characteristics.

https://doi.org/10.1017/S1759078722001258 Published online by Cambridge University Press

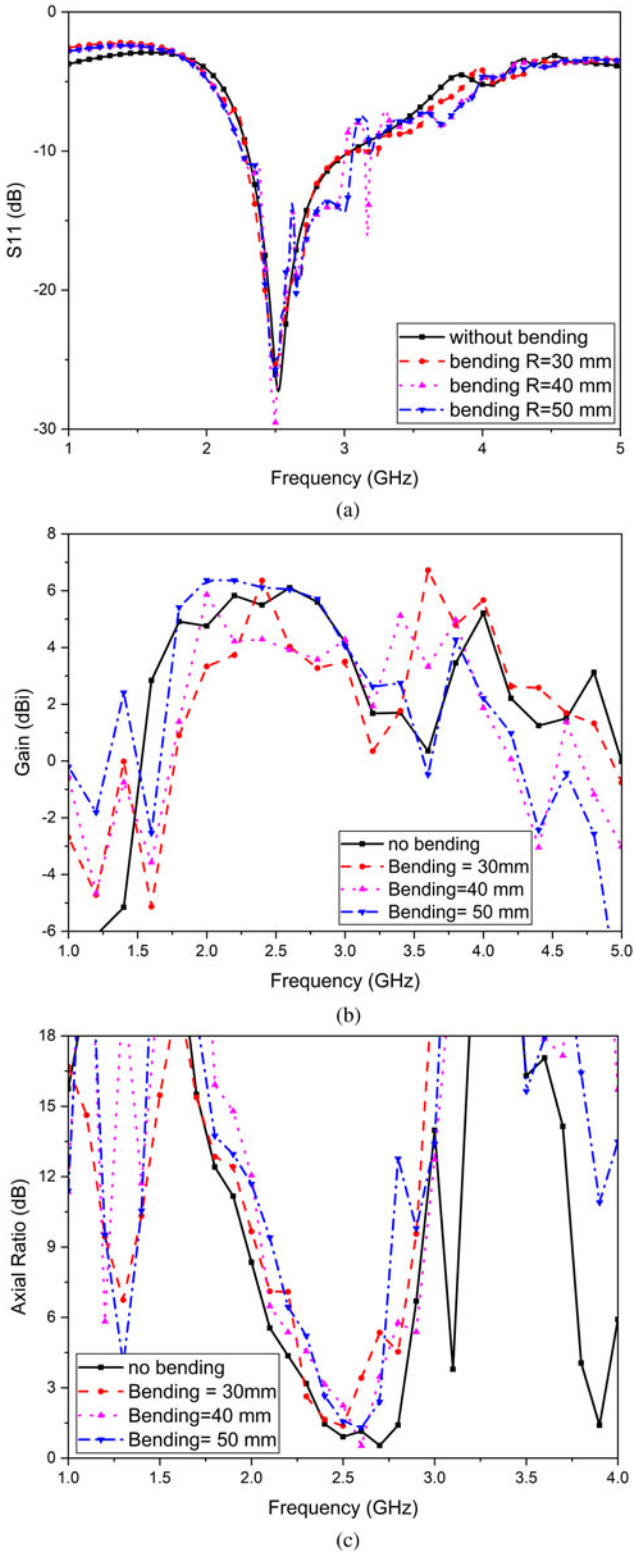

Fig. 6. Simulated (a) S_{11}. (b) Gain. (c) Axial ratio of AMC antenna under different conformal cylinder radius.

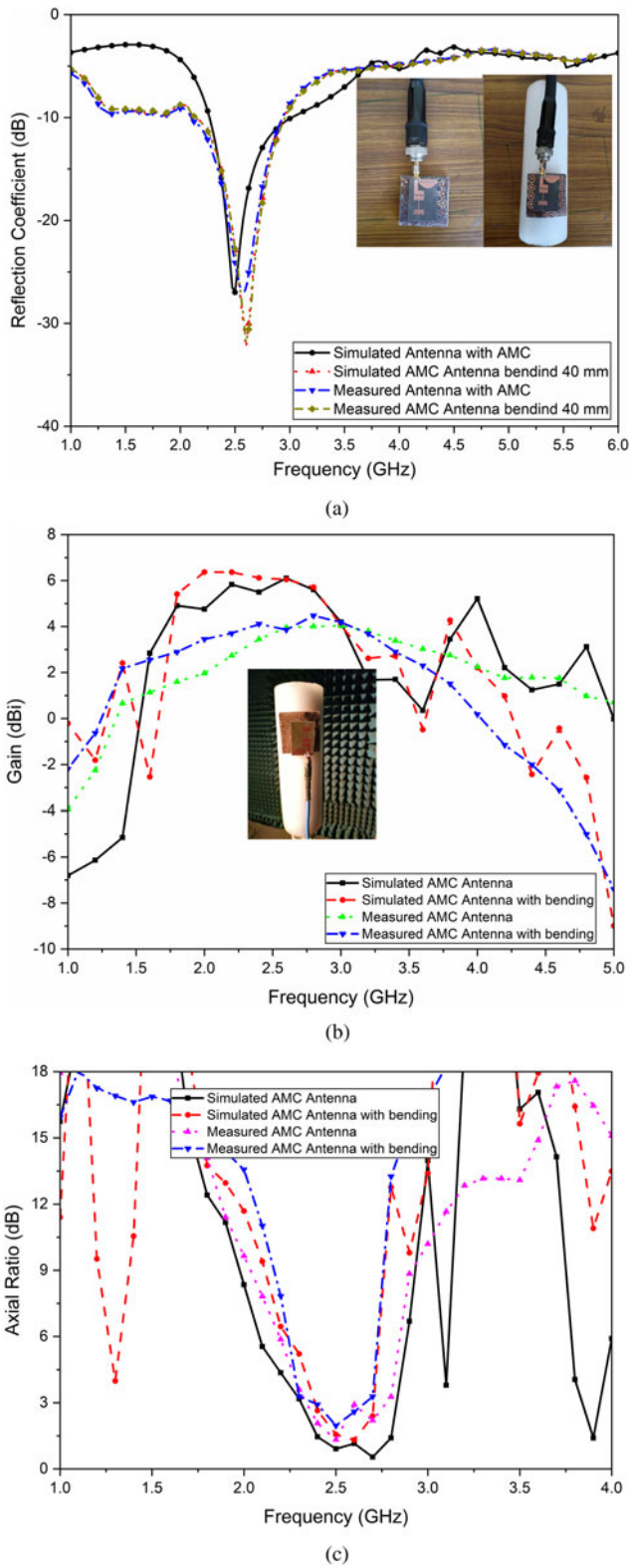

Fig. 7. Simulated and measured (a) S_{11}. (b) Gain. (c) Axial ratio of AMC antenna under normal and bent condition.

Evaluation of AMC antenna performance under bending conditions

For practical wearable applications, the designed antenna must be able to display robust performance owing to changes in shape caused by the curvature of the human body. Thus, in this section, we have evaluated the performance of proposed AMC antenna by varying its shape as per the requirement. The different AMC antenna combinations under conformal conditions placed on

https://doi.org/10.1017/S1759078722001258 Published online by Cambridge University Press

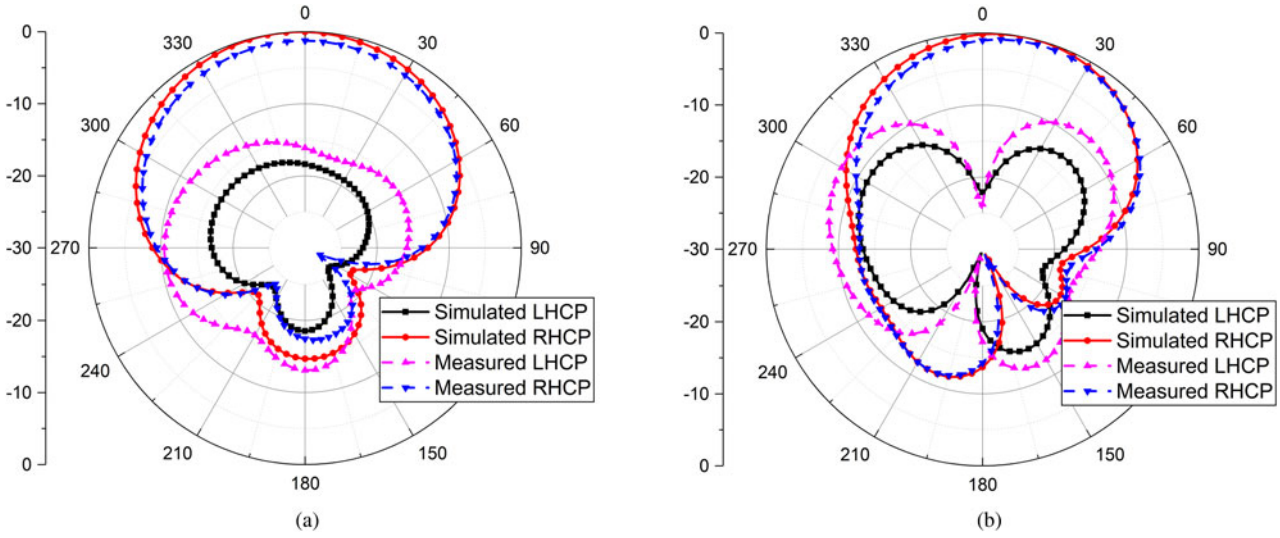

Fig. 8. Normalized LHCP and RHCP radiation pattern of AMC antenna under normal condition. (a) Phi = 0°. (b) Phi = 90° at 2.4 GHz.

cylinders of varying diameter is designed. The simulated results show that the antenna's *S*-parameter has minute impact due to variation in sizes, and the antenna is suited for wearable devices. Figure 6(a) shows the simulated reflection coefficients of AMC antenna under different bending conditions and it is observed that impedance bandwidth of AMC antenna almost remain same for $R = 30$, 40, and 50 mm bending diameter. The simulated gain of the antenna for bending $R = 30$, 40, and 50 mm is shown in Fig. 6(b); it is observed that as the gain of the antenna reduces, bending diameter reduces. The axial ratio of the AMC antenna is shown in Fig. 6(c) and 3 dB ARBW reduces to 2.35–2.6 GHz for $R = 30$ mm. It is clear that as bending level increases, the performance of the antenna slightly deteriorates.

Experimental results and discussion

To investigate the bending performance, proposed antenna is positioned on a cylinder (radius = 50 mm) made up of foam material. The radius of foam cylinder is deliberately selected to mimic the antenna's conformation to a typical human arm. Figure 7 shows the photographs of measurement of AMC antenna using vector network analyzer. The measured and simulated S_{11} of the antenna are shown in Fig. 7(a). It is observed that the measured bandwidth of AMC antenna is 2.3–3.2 GHz with relative impedance bandwidth of 21%. However, the performance of antenna slightly changes in the conformal shape as the human arm of radius is 50 mm. It is seen that impedance bandwidth of AMC antenna with bending is 2.32–3.1 GHz. Therefore, it is clear that antenna has little effect of bending and is suitable for wearable application. Figure 7(b) shows the simulated and measured gain of the antenna, it is observed that the proposed antenna exhibits stable gain in both planar and conformal forms with peak gain of 5.89 and 5.72 dBi in planar and conformal form, respectively. The axial ratio of the proposed antenna is shown in Fig. 7(c), AMC antenna have 3 dB ARBW of 2.36–2.78 GHz, while 3 dB ARBW of bent AMC antenna is 2.38–

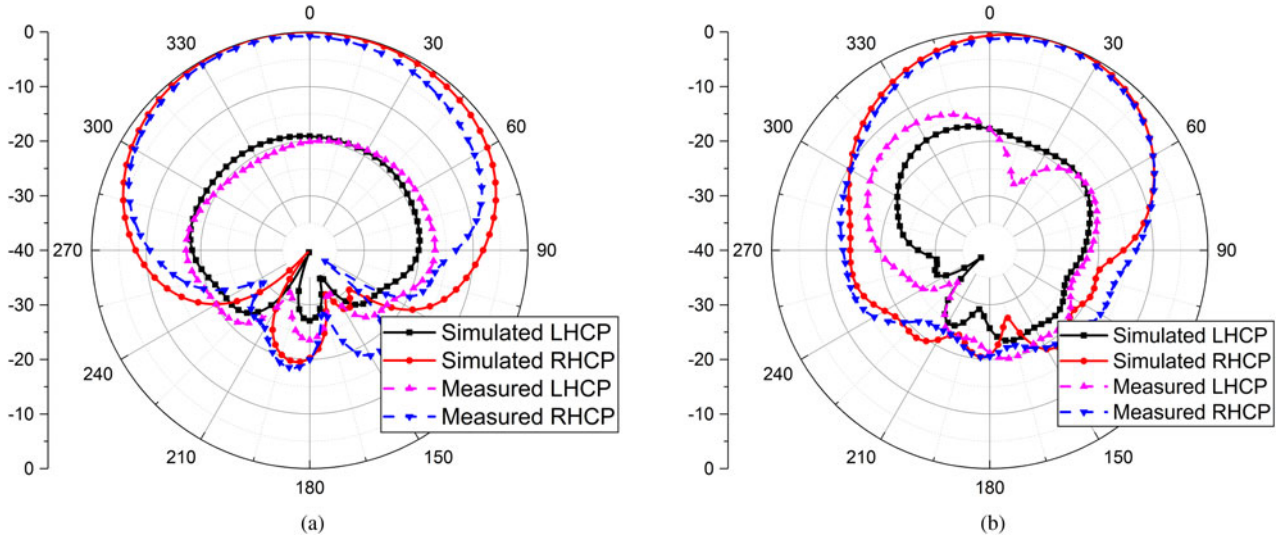

Fig. 9. Normalized LHCP and RHCP radiation pattern of AMC antenna under bent condition. (a) Phi = 0°. (b) Phi = 90° at 2.4 GHz.

https://doi.org/10.1017/S1759078722001258 Published online by Cambridge University Press

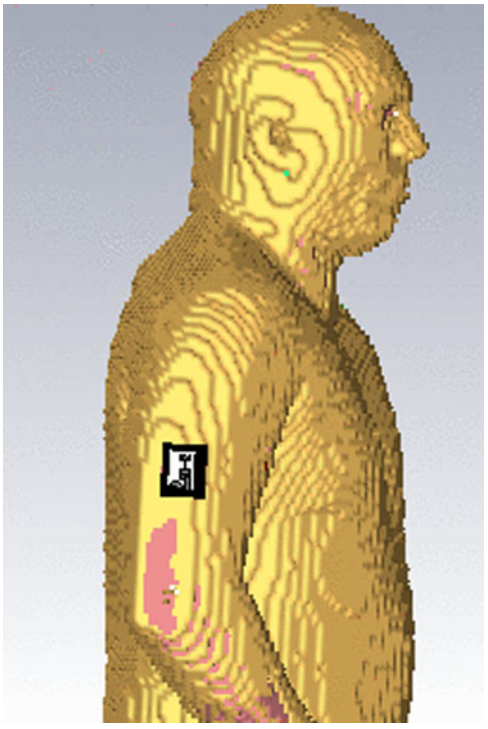

Fig. 10. 3-D CST human body model (Hugo).

2.67 GHz. Further, the normalized radiation patterns of antenna at 2.4 GHz under normal and bent conditions are plotted in Figs 8 and 9, respectively. It has been observed that the proposed antenna LHCP pattern is 15 dB below in comparison with RHCP pattern in the boresight direction. It is seen that HPBW of the AMC antenna and bent AMC antenna is 52° and 45° in phi = 0° plane while HPBW of the AMC antenna and bent AMC antenna is 42° and 41° in phi = 90° plane. Therefore, it is clear that AMC antenna shows stable results in bent form also.

Performance of the proposed antenna on the human body

We have executed full-wave simulations with the designed antennas close to a human body model to verify the on-body performance by using human phantom model named Hugo (from CST MWS voxel family). The proposed antenna is placed on the arm of human body phantom as shown in Fig. 10. Instead of modeling the antenna on the complete numerical body model, a reasonable region of Hugo's arm is chosen for simulation to shorten simulation time. In all the studied scenarios, antenna is assumed to be separated from the skin layer by an additional distance of 2 mm to account for clothing.

The comparison of simulation results of reflection coefficients of the proposed antenna in free space and with human body model (Hugo) is shown in Fig. 11(a). It is observed that impedance of the proposed antenna is slightly shifted to right side and small bandwidth widening is seen with −10 dB impedance bandwidth of 2.32–3.23 GHz due to the loading of human phantom model and impedance matching of the antenna is also reduced. The reduction is due to high dielectric constant values of different tissue layers of human body model. The gain values of the proposed antenna are shown in Fig. 11(b), and it is seen that implementation of human body model has little impact on

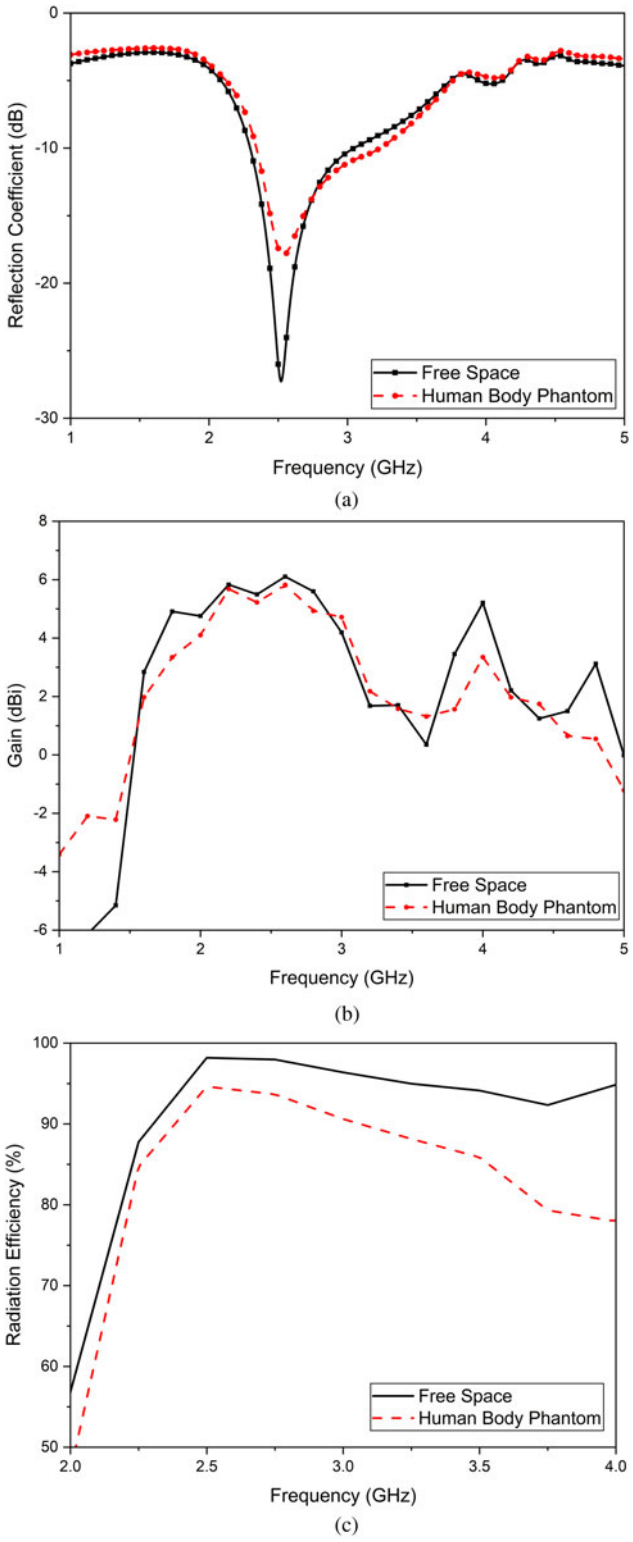

Fig. 11. Simulated results of the proposed antenna in free space and with human body phantom. (a) Reflection coefficient. (b) Gain. (c) Radiation efficiency.

antenna gain and radiation efficiency performance. The simulated peak gain of the antenna is reduced to 5.82 as compared to 6 dBi in free space. The radiation efficiency of the proposed antenna is shown in Fig. 11(c) and we can say that radiation efficiency of the antenna is above 85% in the whole impedance bandwidth for both

https://doi.org/10.1017/S1759078722001258 Published online by Cambridge University Press

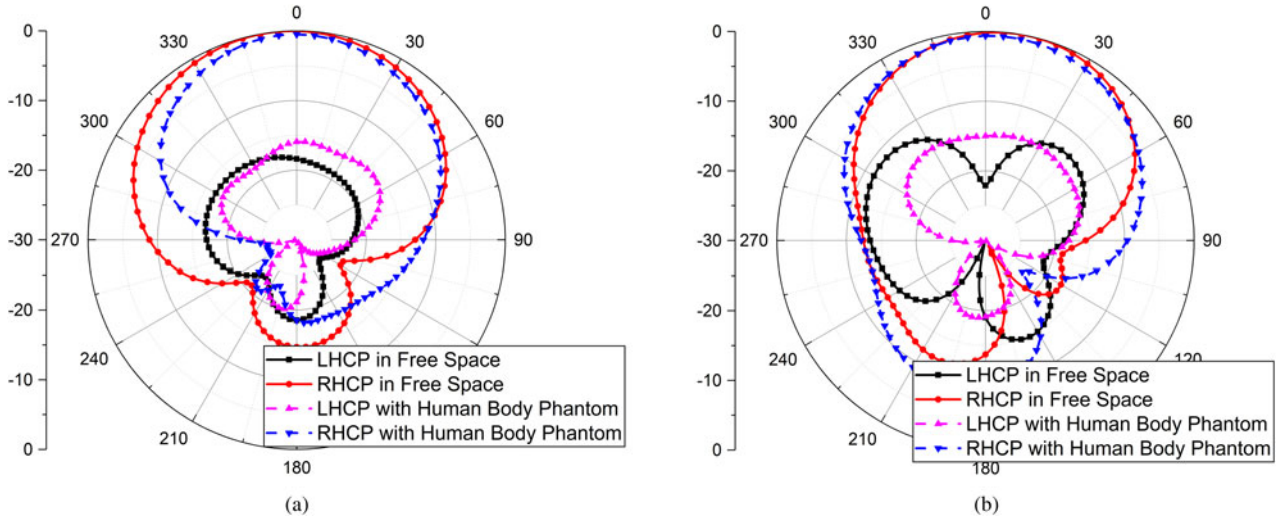

Fig. 12. Simulated normalized radiation patterns of the proposed antenna in free space and with human body phantom. (a) Phi = 0°. (b) Phi = 90°.

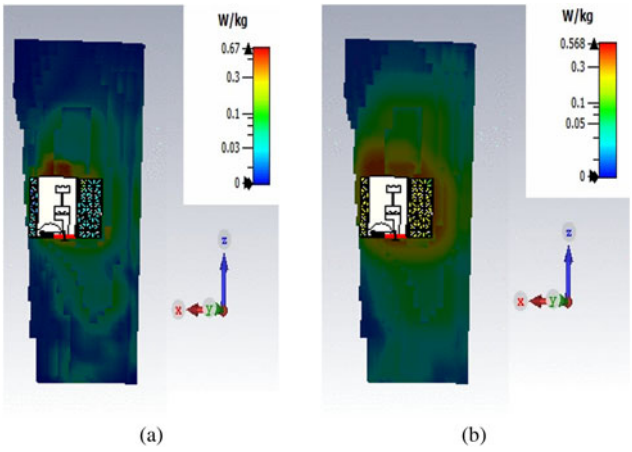

Fig. 13. SAR simulation. (a) 1 g human tissue. (b) 10 g human tissue at 2.4 GHz.

the cases. Figure 12 shows the simulated radiation patterns of the proposed antenna in free space and with human body condition at 2.4 GHz. The results illustrate that radiation characteristics of antenna change trivially between free space and on-body status because of the good isolation achieved by the AMC structure.

SAR results of proposed antenna for wearable safety

To guarantee compliance with safety laws, the SAR level of a wearable antenna must be evaluated while designing the antenna. Furthermore, SAR is used to assess the risks that wearable antennas pose to human health. Thus, the RF energy received by human tissues must not go over the critical threshold of 1.6 W/kg for any 1 g tissue or 2 W/kg for 10 g tissue, according to the IEEE C95.1-1999 and IEEE C95.1-2005 standards. The AMC antenna is placed on the CST human body model (Hugo) to assess the SAR of the human body. Figure 10 depicts the numerical simulation of a 3-D body with approximate human tissue data. After loading the AMC structure, the EM wave radiation to the human body is effectively reduced. Figure 13 depicts the simulated SAR distribution on human hand. From Fig. 13(a) it is seen that at 2.4 GHz, the maximum value of SAR is 0.67 W/kg of 1 g/m^3 under the condition of 1 W input power. Further, Fig. 13(b) depicts the SAR distribution for 10 g human body tissue and it is observed that peak SAR value is 0.568 W/kg of 10 g/m^3.

Table 2 depicts the SAR simulation at 2.4 GHz, as shown in the table below. The AMC antenna's assessed SAR values are all considerably below the regulated SAR criteria, but the monopole antenna does not. The reason for this is that antenna without AMC produces an omnidirectional pattern, but an AMC antenna produces a directing radiation pattern. The SAR study demonstrates the AMC antenna's advantage for operating close to the human body. A comparison of the proposed work with the work discussed in literature is presented in Table 3. It is seen

Table 2. SAR analysis of antennas at 2.4 GHz (1 g tissue (w/kg))

Antennas	*E*-plane	*H*-plane
Antenna without AMC	41.25	42.32
Antenna with AMC	0.67	0.56
Antenna with AMC bent	0.52	0.68

Table 3. Comparison of the proposed work with the previous work

Ref	Impedance bandwidth (GHz)	Gain (dBi)	Polarization	Size (λ^2)
Proposed	2.3–3.1	5.89	Circular	0.38 × 0.38
[25]	2.28–2.51, 5.2–6	6.2	Linear	0.68 × 0.68
[24]	4.30–5.90	6.12	Linear	1.47 × 0.97
[23]	2.425–2.47	0.12	Linear	0.4 × 0.4
[19]	2.4–2.5	0.95	Linear	1.02 × 0.7
[16]	2.4 and 5.8	–	Linear	0.8 × 0.8
[15]	5.15–5.87	–	Linear	0.17 × 0.17

https://doi.org/10.1017/S1759078722001258 Published online by Cambridge University Press

that the proposed antenna has smaller foot print with stable gain as compared to the work reported. The proposed AMC antenna exhibits circular polarization which makes it a good candidate for ISM band wearable applications.

Conclusion

A CRLH-TL-inspired compact CP antenna is presented. For wearable antenna applications, the proposed CP antenna is backed by an AMC-based metasurface. The developed AMC antenna has an impedance bandwidth of 21% (2.3–3.2 GHz) and a gain of 5.89 dBi. Numerical calculations and experimental results have also demonstrated that the designed AMC-based antenna works well in terms of radiation performance in conditions of minor modifications due to structural deformation such as bending, as well as human body loading effects. Furthermore, the AMC reflector significantly minimizes SAR values, making the AMC antenna performance better than a single CRLH-TL-based CP antenna.

Data. The datasets generated during and/or analyzed during the current study are available from the corresponding author on reasonable request.

Acknowledgements. Special thanks to Prof. Binod Kumar Kanaujia, NIT, Jalandhar for support this work.

Author contributions. All authors contributed to the study conception and design. Software simulation and analysis were performed by Mohammad Hussain Abbas and Ankit Sharma. The first draft of the manuscript was written by Mohammad Hussain Abbas and the manuscript was revised by Deepak Gangwar and Shamsher Singh. All authors read and approved the final manuscript.

Financial support. None.

Conflict of interest. None.

References

1. **Haga N, Saito K, Takahashi M and Ito K** (2009) Characteristics of cavity slot antenna for body-area networks. *IEEE Transactions on Antennas and Propagation* **57**, 837–843.
2. **Halland PS and Hao Y** (2012) *Antennas and Propagation for Body-Centric Wireless Communications*. Artech House, https://uk.artechhouse.com/Antennas-and-Propagation-for-Body-Centric-Wireless-Communications-Second-Edition-P1466.aspx
3. **Zu H-R, Wu B and Zhang Y-H** (2020) Circularly polarized wearable antenna with low profile and low specific absorption rate using highly conductive graphene film. *IEEE Antennas and Wireless Propagation Letters* **19**, 2354–2358.
4. **Arif A, Zubair M, Ali M, Khan MU and Mehmood MQ** (2019) A compact, low-profile fractal antenna for wearable on-body WBAN applications. *IEEE Antennas and Wireless Propagation Letters* **18**, 981–985.
5. **Pei R, Leach M, Lim EG, Wang Z, Wang J, Wang Y, Jiang Z and Huang Y** (2020) Wearable EBG-backed belt antenna for smart on-body applications. *IEEE Transactions on Industrial Informatics* **16**, 7177–7189.
6. **Joshi R, Hussin EFNM, Soh PJ, Jamlos MF, Lago H, Al-Hadi AA and Podilchak SK** (2020) Dual-band, dual-sense textile antenna with AMC backing for localization using GPS and WBAN/WLAN. *IEEE Access* **8**, 89468–89478.
7. **Sambandam P, Kanagasabai M, Ramadoss S, Natarajan R, Alsath MG, Shanmuganathan S, Sindhadevi M and Palaniswamy SK** (2020) Compact monopole antenna backed with fork-slotted EBG for wearable applications. *IEEE Antennas and Wireless Propagation Letters* **19**, 228–232.
8. **Gao G, Yang C, Hu B, Zhang R and Wang S** (2019) A wide-bandwidth wearable all-textile PIFA with dual resonance modes for 5 GHz WLAN applications. *IEEE Transactions on Antennas and Propagation* **67**, 4206–4211.
9. **Foroozesh A and Shafai L** (2011) Investigation in to the application of artificial magnetic conductors to bandwidth broadening, gain enhancement and beam shaping of low profile and conventional monopole antennas. *IEEE Transactions on Antennas and Propagation* **59**, 4–20.
10. **Zhu S and Langley R** (2009) Dual-band wearable textile antenna on an EBG substrate. *IEEE Transactions on Antennas and Propagation* **57**, 926–935.
11. **Raad HR, Abbosh AI, Al-Rizzo HM and Rucker DG** (2013) Flexible and compact AMC based antenna for telemedicine applications. *IEEE Transactions on Antennas and Propagation* **61**, 524–531.
12. **Zhang Y, von Hagen J, Younis M, Fischer C and Wiesbeck W** (2003) Planar artificial magnetic conductors and patch antennas. *IEEE Transactions on Antennas and Propagation* **51**, 2704–2712.
13. **Kern DJ, Werner DH, Monorchio A, Lanuzza L and Wilhelm MJ** (2005) The design synthesis of multiband artificial magnetic conductors using high impedance frequency selective surfaces. *IEEE Transactions on Antennas and Propagation* **53**, 8–17.
14. **Ashyap AYI, Dahlan SHB, Zainal Abidin Z, Abbasi MI, Kamarudin MR, Majid HA, Dahri MH, Jamaluddin MH and Alomainy A** (2020) An overview of electromagnetic band-gap integrated wearable antennas. *IEEE Access* **8**, 7641–7658.
15. **Mantash M, Tarot AC, Collardey S and Mahdjoubi K** (2016) Design methodology for wearable antenna on artificial magnetic conductor using stretch conductive fabric. *Electronics Letters* **52**, 95–96.
16. **Yan S, Soh PJ and Vandenbosch GA** (2014) Low-profile dual-band textile antenna with artificial magnetic conductor plane. *IEEE Transactions on Antennas and Propagation* **62**, 6487–6490.
17. **Gao G, Zhang R-F, Geng W-F, Meng H-J and Hu B** (2020) Characteristic mode analysis of a nonuniform metasurface antenna for wearable applications. *IEEE Antennas and Wireless Propagation Letters* **19**, 1355–1359.
18. **Ramadan M and Dahle R** (2019) Characterization of 3-D printed flexible heterogeneous substrate designs for wearable antennas. *IEEE Transactions on Antennas and Propagation* **67**, 2896–2903.
19. **Kim S, Ren Y, Lee H, Rida A, Nikolaou S and Tentzeris MM** (2012) Monopole antenna with inkjet-printed EBG array on paper substrate for wearable applications. *IEEE Antennas and Wireless Propagation Letters* **11**, 663–666.
20. **Agarwal K, Guo Y and Salam B** (2016) Wearable AMC backed near endfire antenna for on-body communications on latex substrate. *IEEE Transactions on Components, Packaging and Manufacturing Technology* **6**, 346–358.
21. **Rizwan M, Khan MWA, Sydänheimo L, Virkki J and Ukkonen L** (2017) Flexible and stretchable brush-painted wearable antenna on a three-dimensional (3-D) printed substrate. *IEEE Antennas and Wireless Propagation Letters* **16**, 3108–3112.
22. **Catarinucci L, Chietera FP and Colella R** (2020) Permittivity-customizable ceramic-doped silicone substrates shaped with 3-D-printed molds to design flexible and conformal antennas. *IEEE Transactions on Antennas and Propagation* **68**, 4967–4972.
23. **Alemaryeen A and Noghanian S** (2019) On-body low-profile textile antenna with artificial magnetic conductor. *IEEE Transactions on Antennas and Propagation* **67**, 3649–3656.
24. **Lai J, Wang J, Sun W, Zhao R and Zeng H** (2022) A low profile artificial magnetic conductor based tri-band antenna for wearable applications. *Microwave and Optical Technology Letters* **64**, 123–129.
25. **Khajeh-Khalili F, Shahriari A and Haghshenas F** (2021) A simple method to simultaneously increase the gain and bandwidth of wearable antennas for application in medical/communications systems. *International Journal of Microwave and Wireless Technologies* **13**, 374–380.
26. **Kumar A, De A and Jain RK** (2022) Circular polarized two-element textile antenna with high isolation and polarization diversity for wearable applications. *International Journal of Microwave and Wireless Technologies*, 1–9. doi: 10.1017/S1759078722000332.
27. **Lin Z, Liu R, Wang X, Zheng H, Wang M and Li E** (2020) Metasurface: changing polarization from linear to circular for airborne antenna. *AEU-International Journal of Electronics and Communications* **116**, 153086.
28. **Liu R, Zhang K, Li Z, Cui W, Liang W, Wang M, Fan C, Zheng H and Li E** (2021) A wideband circular polarization implantable antenna for health monitor microsystem. *IEEE Antennas and Wireless Propagation Letters* **20**, 848–852.

https://doi.org/10.1017/S1759078722001258 Published online by Cambridge University Press

29. **Ameen M and Chaudhary RK** (2020) A compact circularly polarized antenna using CRLH inspired transmission line and coupled ring resonator. *AEU-International Journal of Electronics and Communications* **121**, 153238.
30. **Ameen M and Chaudhary RK** (2019) Metamaterial-based wideband circularly polarised antenna with rotated V-shaped metasurface for small satellite applications. *Electronics Letters* **55**, 365–366.

Mohammad Hussain Abbas is currently pursuing Ph.D. in electronics engineering from the University Institute of Engineering and Technology, Maharshi Dayanand University, Rohtak, India. At present his research interest includes metasurfaces, THz antennas, circularly polarized antennas, reconfigurable antennas, and radar cross section reduction of antennas.

Dr. Shamsher Singh earned M.Sc. in electronics in very-large-scale integration (VLSI) and instrumentation engineering in 2002 from Kurukshetra University, Kurushetra, India, and also earned M.Tech. in electronics and communications engineering in 2006, and a Ph.D. in electronics engineering from Maharshi Dayanand University (MDU), Rohtak, Haryana, India. He is currently working as an assistant professor with the Department of Electronics and Communication Engineering, MDU, Rohtak. He has published more than 20 research papers in refereed international journals and conferences. He had supervised several M.Tech. and B.Tech. students in the field of microwave and VLSI designing. His current research interest includes VLSI designing, instrumentation, metasurfaces, circularly polarized antennas and radar cross section reduction of antennas.

Ankit Sharma earned B.Tech. in electronics & instrumentation engineering, in 2008, and an M.Tech. in signal processing, in 2012 from Ambedkar Institute of Advanced Communication Technologies and Research, Delhi, India and a Ph.D. in electronics engineering from Indian Institute of Technology (Indian School of Mines), Dhanbad, India. He is currently working as an associate professor with the Department of Electronics and Communication Engineering, Galgotias College of Engineering and Technology, Greater Noida. He has published more than 20 research papers in refereed international journals and conferences. He had supervised several M.Tech. and B.Tech students in the field of radio frequency and microwave engineering. His current research interest includes metamaterials, metasurfaces, THz antennas, circularly polarized antennas, characteristics mode analysis, substrate integrated waveguides, reconfigurable antennas, and radar cross section reduction of antennas.

Deepak Gangwar earned B.Tech. from Uttar Pradesh Technical University, Lucknow, India, in 2008, and an M.Tech. from Guru Gobind Singh Indraprastha University, Delhi, India in 2011. He obtained a Ph.D. in electronics engineering from Indian Institute of Technology (Indian School of Mines), Dhanbad, India. Currently, he is working as professor in Bharati Vidyapeeth's College of Engineering, New Delhi, India. His research interest includes metamaterial-based antennas, ultra-wideband antennas, metamaterial filters, frequency selective surface, metasurface, and radar cross section reduction.

https://doi.org/10.1017/S1759078722001258 Published online by Cambridge University Press